

A Compact, Lightweight and Singularity-Free Wrist Joint Mechanism for Humanoid Robots

Cornelius Klas, Tamim Asfour

Abstract—Building humanoid robots with properties similar to those of humans in terms of strength and agility is a great and unsolved challenge. This work introduces a compact and lightweight wrist joint mechanism that is singularity-free and has large range of motion. The mechanism provides two degrees of freedom (DoF) and was developed for integration into a human scale humanoid robot arm. It is based on a parallel mechanism with rolling contact joint behaviour and remote actuation that facilitates a compact design with low mass and inertia. The mechanism’s kinematics along with a solution of the inverse kinematics problem for the specific design, and the manipulability analysis are presented. The first prototype of the proposed mechanism shows the possible integration of actuation, sensing and electronics in small and narrow space. Experimental evaluations shows that the design feature unique performance regarding weight, speed, payload and accuracy.

I. INTRODUCTION

Previous work in construction and maintenance of our robots ARMAR-III [1], ARMAR-4 [2] and ARMAR-6 [3] has shown that building humanoid robots with mechanical properties similar to those of humans or even chimpanzees [4] in terms of strength and agility remains a major and unsolved challenge. Despite advances in actuator and sensor technology, this can also be seen in comparison with human motion and other humanoid robots. This is remarkable since electric motors can have a higher power density (1 kW/kg [5] to 7 kW/kg [6]) than human muscles (0.2 kW/kg [7]). One of the reasons for the challenge of achieving human performance is that with many DoF required in humanoid arms and heavy geared transmissions placed in the joint axis, all subsequent joints in the kinematic chain contribute to large inertia for the previous joints, requiring even larger and heavier gears. Robot designs that focus on modularity, scalability and large payloads instead of high accelerations like Centauro [8], HRP-5P [9] or ARMAR-6 [3] use a serial kinematics with direct actuator placement at most joints. Designing a robot as a combination of sensor-actuator-control units (SAC units) offers many advantages especially modularization and reduced complexity, but does not allow for human accelerations due to the large inertia both within the units and across the kinematic chain. Additionally, anthropomorphic design with human-like appearance is more difficult with direct actuator placement in the wrist. Therefore, the following work is focused on remote actuation, i.e.

This work has been supported by the Carl Zeiss Foundation through the JuBot project.

The authors are with the High Performance Humanoid Technologies Lab, Institute for Anthropomatics and Robotics, Karlsruhe Institute of Technology (KIT), Germany {cornelius.klas@kit.edu, asfour}@kit.edu

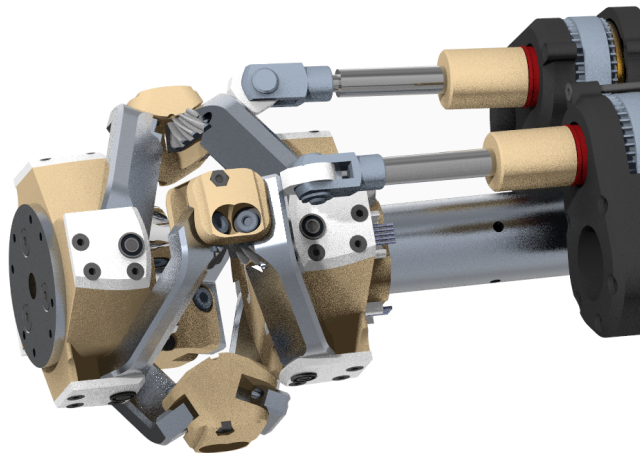


Fig. 1: Rendering of the novel singularity free wrist joint mechanism with large range of motion for humanoid robots.

distant actuator placement.

There are many approaches to articulated mechanisms using cables [10], [11], belts [12] and differential gears [13], [14], levers, or hydraulic systems [15] to position the actuators closer to the center of the body to reduce inertia. A challenge here is the design of the different joints with the necessary transmission of mechanical or electrical energy and control signals. All together, since all existing solutions have their limitations, a compact, powerful and lightweight mechanism is still needed for a human performance in humanoid robots. The proposed mechanism is first designed for the wrist, one of the most difficult joints due to the high demands on motion range and loads with a very compact design of the human counterpart.

In this paper we present the idea and realization of the first physical prototype of the mechanism, which provides a large range of motion. Over the entire hemisphere of possible orientations, the mechanism is singularity-free, providing sufficient force and speed. The mechanism offers rolling contact joint kinematics, with the momentary center of rotation (CoR) always at the empty center of the mechanism. This allows for easy integration of a 6-axis force-torque sensor and routing of power and signals through the center point.

II. RELATED WORK

A general review of the state of the art in artificial wrist design is given in [16]. For a vision of a new dexterous wrist for the iCub humanoid several mechanisms (Gimbal,

iCub mk.2, Five-Bar, Six-Bar, Omniwrist, Quaternion) are compared in [17], accompanied with plots of Cartesian workspace and combinations of orientation angles, joint coordinates and Cartesian coordinates but without the focus on mechatronic realisation.

The following state of the art is limited to wrist designs for versatile and fast manipulation in a limited, human size construction space with remote actuator placement. Some mechanism excluded from the comparison are described in the following: The ARMAR-6 wrist [18] can be used as example for serial kinematic with direct actuator placement. It uses 2 sensor-actor-controller (SAC) units, where the actuation of one is transmitted by gears. Electrical energy and signals are feed through a slip ring which results in a flexion/extension (directions in Fig. 2) range of $\pm 90^\circ$ and a deviation range of $\pm 40^\circ$. The Blue robot [13] is composed of a roll joint and 3 equal 2 DoF units and presents an interesting approach in terms of modularity. The wrist of this arm is not listed in Table I because the rotation axes are in roll, pitch and roll direction, which leads to singularities in the initial end-effector (EEF) position and makes a direct yaw motion of the EEF not possible. For a yaw motion of the EEF the whole forearm has to be rotated by 90° first. A 2 DoF, parallel kinematics and cable driven wrist with plots of maximum joint torques in different orientations is proposed in [19]. It can't be found in our table as well as the shadow hand [20] because they are not yet included in the design of a full humanoid robot. In the DLR Hand Arm System [21] a complex double parallelogram structure allows for cable routing and is actuated by 4 variable stiffness actuators (VSA), however no range of motion is given.

A serial kinematics with remote actuator placement is realized in the ARMAR-III [22] and ARMAR-4 [23] wrist. ARMAR-III uses cables to actuate the first joint and a belt-driven universal joint to actuate the second, where the universal joint limits the motion range of this joint to $\pm 40^\circ$. In ARMAR-4 an arched and belt driven rail in the first joint enables a large range of motion in a very compact design. The second joint is actuated by bowden cables, whose bending by the first joint induces backlash in the system. A differential drive with bevel gears is used in the iCub wrist [14] where the first uses cables and the second belts for actuator placement in the forearm.

Parallel mechanism used in the following wrists offer some advantages: The payload to mass ratio can be larger than 7 for parallel structures [24] while it is typically smaller than 0.15 for serial 6R robots [25]. Also errors and backlash in parallel joints are not added but leveled out. Various parallel mechanisms in general are shown in [25]. The R1 robot wrist [26] offers a tripod kinematics driven by 3 rods which enables a elongation of 130 mm additionally to pitch and roll motions of 30° . In the mobile dual-arm robot AILA [27] one point of a triangle arrangement is fixed by a universal joint while the two other points are actuated by two spindle driven rods. In the RoboRay hand a complex 2 DoF wrist joint including wires for the finger motion is proposed [28]. Two spindles drive a parallel mechanism which results in rolling

TABLE I: Specifications of Wrist Design Examples

Robot	Kin.	Actuators	Range ($^\circ$) fl./ext. dev.	Feed- through
ARMAR-III	univ. j.	2 (belt, cable)	$\pm 60 \pm 30$	no
ARMAR-4	serial	2 (belt, cable)	$\pm 90 \pm 40$	no
iCub [17]	diff.	2 (tendons)	$\pm 56 \pm 38$	yes
R1 [26]	tripod	3 (rods)	$\pm 30 \pm 30$	yes
Aila [27]	tripod	2 (rods)	$\pm 45 \pm 15$	yes
RoboRay[28]	parallel	2 (rods)	$\pm 90 \pm 45$	yes
LIMS2 [30]	parallel	2 (4 cables)	$\pm 90 \pm 90$	yes
Surrogate III*	parallel	2 (pistons)	$\pm 95 \pm 95$	yes
Proposed wrist	parallel	2 (rods)	$\pm 90 \pm 90$	yes

* The Omniwrist III was not yet included in the small space of a humanoid wrist, but in the shoulder joint of Robotic Surrogate III [31].

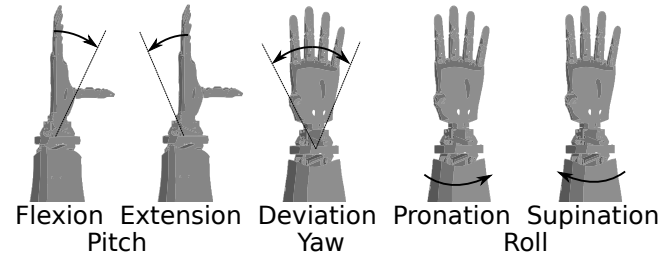


Fig. 2: Wrist motion directions.

contact joint motions in flexion/extension direction and normal rotation in deviation direction. In the LIMS2-Ambidex robot an impressive tendon driven parallel kinematic wrist mechanism [11] provides a wide range of motion with a rolling contact joint kinematics. The elongated mechanism is actuated via 2 pairs of cable pulleys and enables feed though of mechanical energy for a following roll joint. The Omniwrist-III [29] kinematics was not implemented into a humanoid wrist yet, but since it is similar to ours it is included to the comparison.

The motion range of the human wrist with a flexion of 76° , extension of -75° and a deviation from -19° to 33° [32] are reached by some systems like ARMAR-4, RoboRay and LIMS2. If we compare to the human wrist we have to consider the extreme flexibility of the human hand, not reachable in robotic systems yet, which has to be compensated by a higher range of motion in a robotic wrist. Direct comparison of payload is difficult because it highly depends on the scale of the joint and on the distance between joint and hand.

To the best of the authors' knowledge, no other existing wrist mechanism can solve all our requirements to get a compact and powerful robot. The proposed design is similar to the Omniwrist-III [29] design with both having 4 pairs of levers, two of which are actuated and both emulate a rolling contact motion. The challenge is to realize this in a light weight design for a humanoid wrist since backlash is a significant problem in compact prototypes of the original design. This is because the symmetry is only maintained by additional lever pairs over a long kinematic chain. To solve this the proposed wrist has an important difference: With additional gears enforcing symmetry, the mechanism operates with only 2 lever pairs leaving the other two pairs

for improvements of stiffness and backlash. Additionally the new mechanism is completely symmetric to the middle plane and a protective ring is added. The LIMS2 kinematic is the humanoid wrist most similar to this work but has some properties not fitting to our requirements: The design is not compact enough, making humanoid segment length difficult and we wanted to avoid a rope hoist mechanism with long transmission cables which introduce backlash and elasticity. The high friction that can occur with wired mechanisms and a long cable routing is also a reason for a different solution.

III. REQUIREMENTS

The main goals for our robot design are the anthropomorphic appearance and human-like performance. Especially high accelerations are important to achieve motions close to human ones. In order to converge towards this goal, several requirements were identified. Because of actuator weight, the joint accelerations occurring in human motions available in our motion database [33] can not be reached with traditional sequential actuation and actuators in the joint axis. Thus and for anthropomorphic appearance the compact mechanism should be remotely actuated, preferably with linear actuation. It should have low masses and low moments of inertia. The mechanism itself should provide two rotational DoF. Integration of an additional rotation (pronation/supination) should be possible to implement a 3 DoF wrist. For easy control, the initial 2 DoF should be actuated by not more than 2 motors. It should allow easy cable routing through the intersection point of the axes to minimize cable motion and bending, and provide the possibility for absolute angle and force sensors integration.

A range of motion of 90° is suitable to compensate for less flexible robot hands. The proposed range of motion is also large enough to meet the needs of future use in elbow and shoulder joints. Singularity free and low backlash motion is also important in robot applications. If used multiple times in one robot arm the characteristic of a constant velocity joint [34] would be beneficial and avoid unnecessary accelerations of the segments. That also means that the two parts of the mechanism are not twisted and allow a closed flexible hull without crease. High, human-like force and torque are also desired but not yet achievable in human dimensions, but they should be sufficient for everyday tasks.

IV. CONCEPT AND KINEMATICS

To meet the requirements, we proposed a rolling contact joint kinematics mechanism. The three main reasons for that are the possibility of a mechanical design with linear actuation, feed-through and improved manipulability.

If a classical rotational joint is actuated by a lever mechanism, a large motion space is occupied and singularities occur at $\pm 90^\circ$. In a rolling contact joint the total required angle of 90° at full deviation is split into two times 45° at P_E and P_B (Fig. 3d), which makes linear actuation with a large range of motion possible. The same effect reduces the bending in cables and transmissions of mechanical energy guided through the mechanisms center.

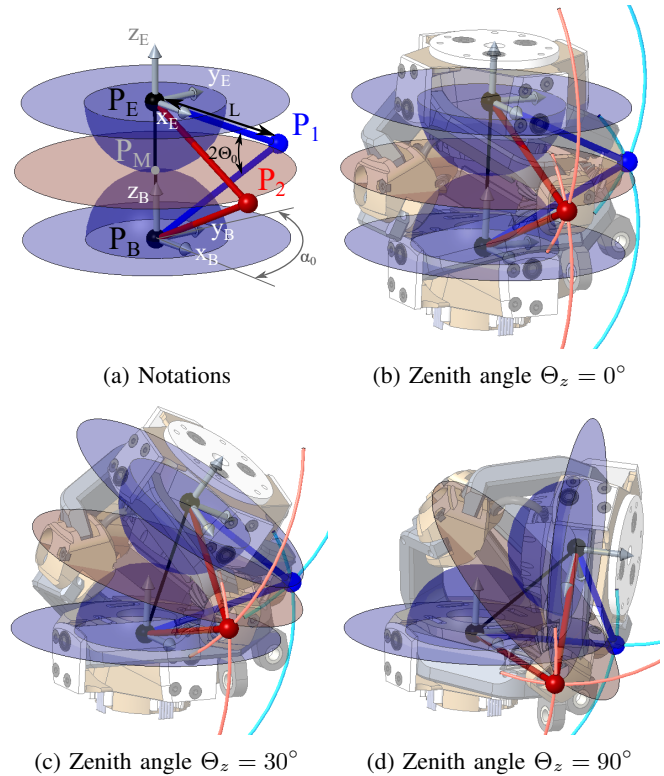


Fig. 3: Visualization of wrist kinematics.

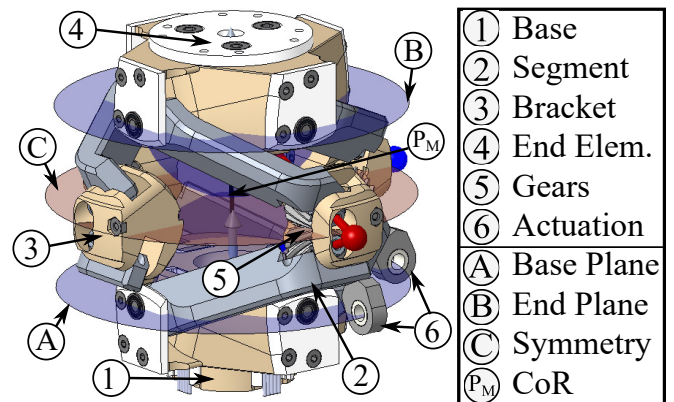


Fig. 4: Essential components of the wrist mechanism.

For the rolling contact joint with additional pronation/supination in [11] the manipulability is much better than for a roll-pitch-roll or roll-pitch-yaw serial arrangement. As it turns out, this also applies to this wrist joint mechanism as shown in Fig. 7. Within the mechanically possible range of motion, there are neither serial singular configurations where the actuators can move while the wrist is at rest neither parallel singularities with nonzero wrist velocities for zero actuator velocities. Such singularity-free kinematics is a great advantage. Another advantage is that parallel kinematics features higher accuracy than serial robots because their errors are averaged instead of added cumulatively [35].

The mechanisms main elements are the *Base* with the coordinate system x_B , y_B and z_B at P_B and the *End*

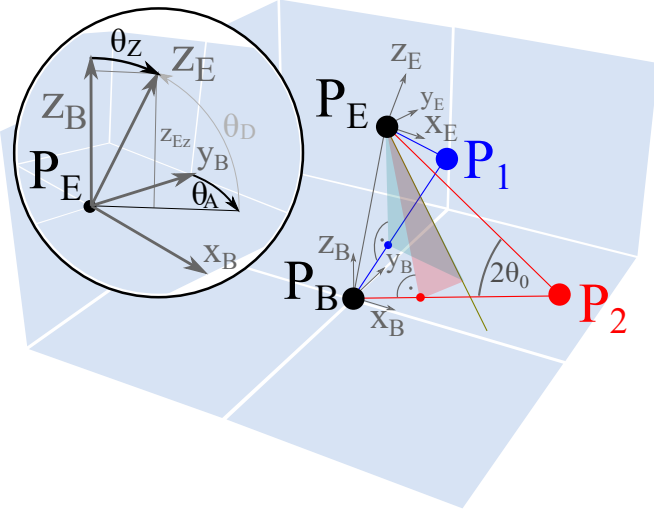


Fig. 5: Derivation of the Forward Kinematics. *End Element* orientation in zenith angle Θ_Z and azimuth angle Θ_A .

Element with the coordinate system x_E, y_E and z_E at P_E which is also the tool center point (TCP) if no hand with its own TCP is added to the wrist. The *base plane* and the *end plane* are the corresponding z -planes. Two actuated segment pairs $\overline{P_B P_1}$ and $\overline{P_1 P_E}$ as well as $\overline{P_B P_2}$ and $\overline{P_2 P_E}$ connect *Base* and *End Element*. Two passive segment pairs are added in the prototype. The kinematic model of the proposed wrist mechanism is shown in Fig. 3 and its essential components are shown in Fig. 4. It has the following properties:

- The mechanism (Fig. 4) with the origin \textcircled{A} and *end plane* \textcircled{B} is symmetric to the *middle plane* \textcircled{C} .
- There are points P_1 and P_2 on the symmetry plane through P_M (Fig. 3). P_1 can only move on a circle around P_B with radius L in the y_B - z_B -plane of the *Base* and on a circle around P_E with radius L in the y_E - z_E -plan of the *End Element*. For P_2 these planes are rotated by a fixed angle α_0 around z .
- There is a fixed angle of $2 \cdot \Theta_0$ between each pair of segments.
- The characteristic values for the complete description of an instance of this mechanism are the segment length L , the angle between the segment pairs of the kinematic chain $2 \cdot \Theta_0$ and the angle between the segment rotation axis α_0 .

With these properties, the mechanism behaves like a rolling contact joint with the CoR P_M at the contact point of virtual spheres connected to the base part $\textcircled{1}$ and the end part or TCP $\textcircled{4}$. The rolling contact joint behavior is enforced in the following way: The points can only move on fixed paths on spheres both around P_B and P_E with P_1 and P_2 always being on the intersection of these paths. The fixed angle Θ_0 ensures a constant distance d between P_E and P_B . Linear actuation of P_1 and P_2 in z -direction can control the position and orientation of the *End Element* in 2 DoF.

The symmetry of the mechanism is realized by a symmetric structure and gears $\textcircled{5}$ between the segments. Part

is not present in the Omniwrist-III mechanism and thus the intersection of the segment axis in one point (P_1, P_2) and the symmetry is not directly guaranteed, but only by the addition of additional segment pairs and introduced over a long kinematic chain.

The limited motions of P_E and P_B is realized by joints between the segments and the *Base* and *End Element* on the *base plane* \textcircled{A} and *end plane* \textcircled{B} . The constant angle between the segments is covered by brackets $\textcircled{3}$ with joints, whose axes intersect in P_1 and P_2 . The attack point of actuation is shifted to $\textcircled{6}$ in the prototype. In contrast to the Omniwrist III design [29], the mechanism is working with only 2 segment pairs. Additional pairs at different angles can be added for improvements of stiffness and backlash. For the prototype and the kinematic shown in Fig. 3 and Fig. 4, an angle α_0 of 90° between the two actuated segments and also for the two additional segment pairs was chosen.

The TCP $\textcircled{4}$ orientation described by x_E, y_E, z_E can be always calculated from its position by exploiting the symmetry of the construction with respect to the middle Plane: Mirroring the x_B and y_B vectors on middle plane results in the x_E and y_E vectors. The z_E vector is mirrored and inverted to keep a right-handed coordinate system. The expression of orientation as azimuth Θ_A and declination Θ_D or zenith angle Θ_Z (Fig. 5) corresponds to the mechanical characteristics of the joint. Since the azimuth angle of z_E is in the same direction as $\overline{P_B P_E}$, it can be calculated as $\Theta_A = \text{atan2}(P_{Ex}, P_{Ey})$. The declination angle $\Theta_D = \text{asin}(z_{Ez})$ can be calculated from z_{Ez} and the zenith angle from $\Theta_Z = \pi/2 - \Theta_D$. The zenith angle has a radially symmetric distribution over the plot of P_{Ex} and P_{Ey} . If the joint mechanism should be used in a kinematics solver, which only allow rotation and translation joints, an equivalent kinematics can be used:

$$\mathbf{Q} = \mathbf{R}_z(-\Theta_A)\mathbf{R}_x(-\Theta_Z/2)\mathbf{T}_z(d)\mathbf{R}_x(-\Theta_Z/2)\mathbf{R}_z(\Theta_A)$$

In the following, we describe the forward and inverse kinematics of the wrists mechanism with the constant angles θ_0 and α_0 , which can vary in different mechanical realizations.

A. Inverse and Forward Kinematics

The aim of inverse kinematics is to come from the TCP coordinates (P_{Ex}, P_{Ey}) or orientation $\mathbf{x}(\Theta_A, \Theta_Z)$ to the linear segment actuation $\mathbf{q}(P_{1z}, P_{2z})$. The TCP orientation can be calculated from the position. In parallel mechanisms the inverse kinematics is typically easier to find then the forward kinematics. The inverse kinematics problem can be solved by constructing the middle plane from $P_E/2$ and intersecting it with the circle of motion of P_1 and P_2 . The needed actuation of the two segments for a certain position of the *End Element* plotted as orange and blue arrows in Figure 6. For the forward kinematics from linear segment actuation \mathbf{q} to TCP coordinates, the intersection of two planes and a sphere in P_E can be used (see Fig. 5).

Manipulability ellipsoids are the mapping of a unit sphere of joint velocities through the Jacobi matrix to an ellipse in the space of joint velocities $\dot{\mathbf{x}} = \mathbf{J}(\mathbf{q}) \cdot \dot{\mathbf{q}}$. The principal axis of the ellipsoid indicate the direction of highest and

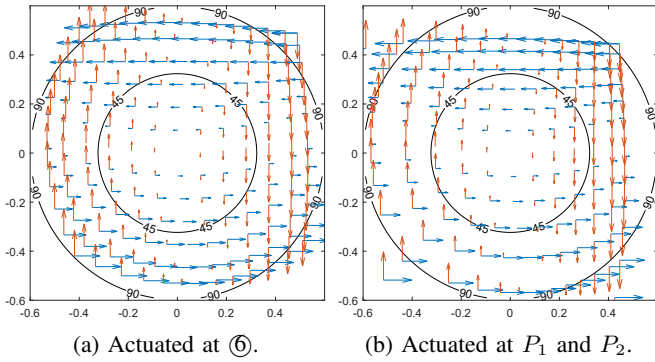


Fig. 6: Inverse kinematics with different points for linear actuation. Circles for the zenith angles of 45° and 90° is plotted in black.

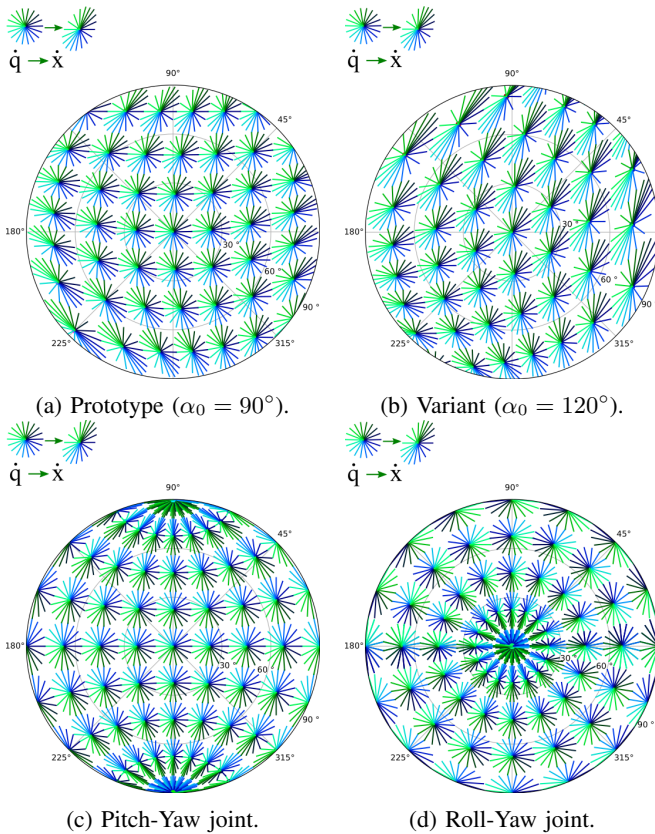


Fig. 7: Azimuth-zenith manipulability ellipsoids for different joints in different joint positions. Singularities occur in Pitch-Yaw and Roll-Yaw joints. There are circles for the zenith angles of 30° , 60° and 90° as well as radial lines every 45° for the azimuth angles.

lowest speed. A degenerated (flat) form of the ellipsoid indicate proximity to a singular configuration. The length of a axis is the scaling factor between joint and TCP velocities in this direction. The angular velocity at different *End Element* orientations of a mechanism that is linear actuated at 6 in z -direction with $\|\dot{\mathbf{q}}\| = 1$ is shown in Fig. 7, with $\dot{\mathbf{q}}$ being the linear actuation speed. The speed ratio from linear actuation to angular velocity is relative constant up to

TABLE II: Mechanical components of the wrist prototype

Comp.	Description
(a)	NEMA17 stepper motor
(b)	MXL 012 mini-pitch belt drive
(c)	Igus DST-JFRM spindle nut
(d)	DST-LS-6P35X5P08-R-ES Spindle
(e)	Bearing with with encoder magnet
(f)	Clevis Joints similar to DIN 71752
(g)	Aluminium tube with internal cabling
(h)	Protective ring
(i)	Jointed motor mount

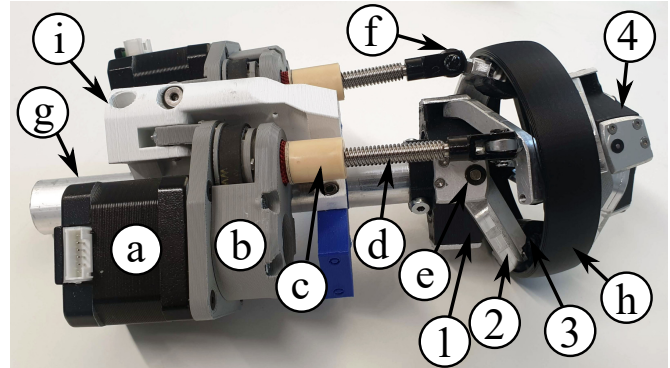


Fig. 8: Prototype of the new wrist mechanism

a zenith angle of 75° . The form and size of the ellipsoids can be adapted to the requirements by changing the angles θ_0 and α_0 as well as the positions of actuation points 6.

V. REALIZATION OF A PROTOTYPE

The concept of the mechanisms has been designed, build and tested for future use as wrist of a humanoid robot arm. For the prototype, an angle $\alpha_0 = 90^\circ$ between the two actuated segment pairs was chosen. Two additional segment pairs in 90° angles are added for improved stiffness. A symmetric design relative to the middle plane (C in Fig. 4) creates space for stiffer segments and bevel gears 5. The gears between all segment pairs enforce this symmetry and prevent skewed axis. The cone form of the bevel gears between the levers enforces the angle of $2 \cdot \Theta_0$. The virtual points P_1 and P_2 are realized as intersection of the bracket axis (Fig. 4, 3) with miniature ball bearings. The 3d printed brackets move on a circle on the middle plane during wrist motion. This allows the installation of a ring, (h in Fig. 8) which could also increase the stiffness in future versions, but here only acts as 3d printed protection. The friction caused by the relative movement of this protective ring with respect to the brackets is negligible, since the relative movement is small and the connection is established with a loose fit.

A. Structure and Actuation

In the construction of the wrist mechanism, we aim at a low weight and low cost design with relatively high stiffness. This was achieved by a combination of 3d printed and milled parts as well as standard components. The main structure is an aluminium tube g in Fig. 8, which allows internal

cabling that is connected to the *base part* ①. It is made from a combination of 3d printed and aluminium parts. The segments ② are milled from aluminum and combined with 3d printed bevel gears (⑤ in Fig. 4) covered by a protective, 3d printed ring (⑥ in Fig. 8). 3d printed brackets (③ in Fig. 4) connect the 4 segment pairs. All joints in the mechanism are plain bearings but can be replaced by F-682-X2Z miniature ball bearings, which fit into the same space.

The prototype of the wrist mechanism is shown in in Fig. 8. It is actuated by 2 NEMA17 stepper motors ④ that drive a MXL 012 mini-pitch belt ⑥, which actuates a Igus DST JFRM spindle nut ⑦. Thus, a linear motion of the Igus DST-LS-6P35X5P08-R-ES spindle ⑧ is generated. The whole actuation is combined in parallel axes with clevis joints similar to DIN 7175 at the actuated segments ⑨ and at the motor mounts ①.

B. Sensing and Electronics

The mechanism can be equipped with several sensors for feedback and control. In the prototype, the space for sensors and required cables in the segment axis is reserved. Relative position is known by counting the steps of the stepper motors. All motors can include incremental encoders that allow precise velocity and position control. For force control an ATI mini 25 6-axis force torque sensor can be mounted recessed in the *End Element* ④. This is very important for a compact design and proximity of hand to the wrist joint center. Force sensors can be included at the motor mount. The 4 base segment joints ③ contain magnets for rotary magnetic encoders. The matching compact and high-speed RLS RM08 sensors designed for use in harsh environments fit into the base ①. Space for electronics is foreseen under the tube on the opposite side of the motors. In the prototype control of the stepper motors is realized with an Arduino board and a suitable CNC-shield. The specification of the wrists prototype is given in Table III.

TABLE III: Specifications of the complete wrist prototype

Total weight	910 g
Mechanism weight	350 g
Motor weight	2 × 280 g
Wrist diameter	8 cm
Footprint	19 cm × 12 cm
Speed	500 °/s
Payload	5 kg

VI. EVALUATION

The design and assembly of the first actuated wrist prototype showed that it is possible to build and assemble this wrist joint mechanism. Experiments showed that it is possible to route all necessary cables and power supply for a humanoid hand through the middle of the joint mechanism, where the cables experience very little length change. A 6-axis force-torque sensor including cables was also embedded into the prototype. Other experiments showed that it is possible to also route flexible shafts through the joint center. The analytical kinematic solution of the forward and inverse

kinematics was validated with a numerical one in Matlab Simulink. In the following evaluation, important parameters are assessed to evaluate the proposed gearbox design.

A. Experimental Setup

For the evaluation experiments, the prototype was fixed to a table while a laser pointer was fixed to the *End Element* (Fig. 9). For experiments including external loads, different weights were attached at a fixed distance to the joint center. The position of the laser point could be read on a distant scale to magnify small angular changes. Due to the large distance, changes in the end element position can be neglected compared to the small angular errors and deflections measured in the experiments. The relative position of the actuated segments in the full motion range could be set by a python interface to the stepper motor controller. For different load and motion directions, the whole prototype was rotated while force and laser stay in floor pointing orientation.

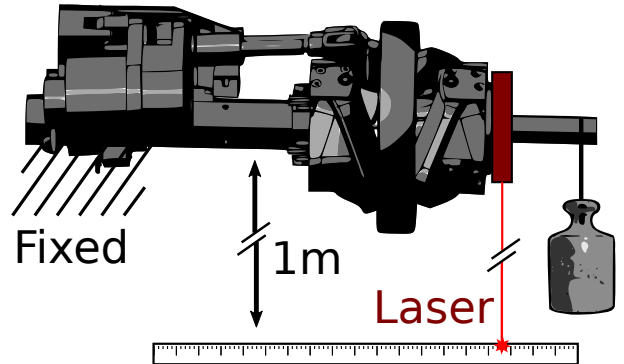


Fig. 9: Experimental setup for evaluation experiments.

B. Mechanical Evaluation

The range of motion of the prototype with feed-through of dummies of all necessary hand supply cables is $\pm 95^\circ$ for the flexion/extension and deviation motion. For the motion diagonal to these directions, the range of motion is $\pm 88^\circ$. If necessary, these values can be increased by smaller bearings or slight changes of the angle θ_0 .

The experiments showed large improvement of the wrist mechanism to a first prototype of the same size but with the Omniwrist III kinematics, which has a axial backlash of 2.5 mm and a angular backlash of 7° . The prototype of the new wrist mechanism is axial backlash free and with a total backlash of 1.7° . For the wrist alone, the angular backlash is reduced to 0.6° . The additional error is mainly caused by the 3d printed motor-spindle system and thus can still be improved in later versions. This means an error of the hand center position in 100 mm distance of about 2.9 mm for the whole mechanism and 1 mm for the wrist alone.

The large difference for the backlash in the occur since the symmetry and the intersection of the lever axis in the Omniwrist III is only introduced over a long kinematic chain by additional segment pairs. A very stiff design of all segments and joints would prevent that but is not possible in

the desired weight and size. Calculations for joint positions near the initial position show, that in a setup without gears, similar to the Omniwrist III design, the maximal radial bearing torques rise up to 16 times the total joint torque. In a setup with gears and an assumed equal load distribution over parallel segment pairs each gear has to take a load of only have the total joint torque and the maximum radial bearing torques drop to 2.5 times the total joint torque.

The elasticity of the complete prototype was measured orthogonal (torque around x and y in Fig. 4) and diagonal. The diagonal stiffness is 1.3 Nm/deg and the orthogonal one 1.4 Nm/deg.

The repeatability for reaching the same angle was tested with 10 repeated rotations. Due to the combined rotation and translation of the mechanism, the given angle is calculated from the error of a point in a distance of 1 m, where the translational error is negligible compared to the rotational error. The mean error around the x axis is 0.2° and 0.1° for rotations around the y axis. For repeated rotations around a diagonal, where both motors are actuated, the error is 0.4° . This means an error of the hand center position of about 0.2 mm to 0.7 mm. With the planed absolute encoders in lever rotation joints, backlash and elasticity can be mostly measured and compensated. The angular static friction in the joint is 0.1 N m. This is important for the accuracy of torque measurement, if torque is measured via actuator force. This is a good value compared to cross roller bearings of a similar size used in serial robots, which have 0.3 N m-3 N m [36] and the LIMS with a friction smaller than 1 N m [11].

Load Experiments with a weight of 5 kg at the at the future hand position were successfully conducted. Higher loads were not possible due to motor power limits and to avoid damage on the mechanical joint parts and bearings, which are designed for these loads.

C. Costs

The 16 aluminium parts and 27 3d printed parts were manufactured in house for material costs of less than 50€. Mechanical parts like belts, bearings and screws for less than 20€ are used. The most expensive parts are threaded spindles and nuts (igus) for together 100€. For actuation and control, stepper motors for 20€ and an arduino with cnc-shield and drivers for 22€ are used. Thus the complete material costs for the fully functional wrist prototype amounts to less than 250€. The final version of the wrist for use in a humanoid robot arm will be equipped with brushless motors, relative and absolute encoders, professional 3d printed parts and ball bearings and therefore it will be more accurate but also more expensive. Thus the proposed design offers possibilities as well for low cost as for high quality applications.

VII. CONCLUSION AND FUTURE WORK

This paper presented the concept, kinematics, mechanical design and hardware realization of a compact, lightweight, singularity free and low cost 2 DoF wrist mechanism for a humanoid robot arm. An analytical solution for forward and inverse kinematics was presented and validated with

a numeric solution. The experimental evaluation showed a functional prototype of the wrist with good performance. The mechanical properties of the prototype were evaluated in terms of payload and accuracy. A PCB for the version of the wrist that will be used in the design of the next generation of our ARMAR robots is currently under development. Based on the prototype presented in this paper it will include support for BLDC motors, absolute and incremental encoders and a 6-axis force-torque sensor.

As next, the integration of the mechanism in a complete humanoid robot arm will be performed and tested. We will work on the optimization of the kinematic parameters of the mechanism to approach human motion characteristics and investigate the possibility of using the joint mechanism for the design of other joints of a humanoid upper body such as shoulder, elbow and neck joints.

REFERENCES

- [1] T. Asfour, K. Regenstien, P. Azad, J. Schroder, A. Bierbaum, N. Vahrenkamp, and R. Dillmann, "Armar-III: An integrated humanoid platform for sensory-motor control," in *2006 6th IEEE-RAS international conference on humanoid robots*. IEEE, 2006, pp. 169–175.
- [2] T. Asfour, J. Schill, H. Peters, C. Klas, J. Bückner, C. Sander, S. Schulz, A. Kargov, T. Werner, and V. Bartenbach, "Armar-4: A 63 dof torque controlled humanoid robot," in *2013 13th IEEE-RAS International Conference on Humanoid Robots (Humanoids)*. IEEE, 2013, pp. 390–396.
- [3] T. Asfour, M. Waechter, L. Kaul, S. Rader, P. Weiner, S. Ottenhaus, R. Grimm, Y. Zhou, M. Grotz, and F. Paus, "Armar-6: A high-performance humanoid for human-robot collaboration in real-world scenarios," *IEEE Robotics & Automation Magazine*, vol. 26, no. 4, pp. 108–121, 2019.
- [4] M. C. O'Neill, B. R. Umberger, N. B. Holowka, S. G. Larson, and P. J. Reiser, "Chimpanzee super strength and human skeletal muscle evolution," *Proceedings of the National Academy of Sciences*, vol. 114, no. 28, pp. 7343–7348, 2017.
- [5] Y. Tanaka, S. Sakama, K. Nakano, and H. Kosodo, "Comparative study on dynamic characteristics of hydraulic, pneumatic and electric motors," in *Fluid Power Systems Technology*, vol. 56086. American Society of Mechanical Engineers, 2013, p. V001T01A037.
- [6] S. Seok, A. Wang, D. Otten, and S. Kim, "Actuator design for high force proprioceptive control in fast legged locomotion," in *2012 IEEE/RSJ International Conference on Intelligent Robots and Systems*. IEEE, 2012, pp. 1970–1975.
- [7] I. W. Hunter and S. Lafontaine, "A comparison of muscle with artificial actuators," in *Technical Digest IEEE solid-state sensor and actuator workshop*. IEEE, 1992, pp. 178–185.
- [8] N. Kashiri, L. Baccelliere, L. Muratore, A. Laurenzi, Z. Ren, E. M. Hoffman, M. Kamedula, G. F. Rigano, J. Malzahn, S. Cordasco, *et al.*, "Centauro: A hybrid locomotion and high power resilient manipulation platform," *IEEE Robotics and Automation Letters*, vol. 4, no. 2, pp. 1595–1602, 2019.
- [9] K. Kaneko, H. Kaminaga, T. Sakaguchi, S. Kajita, M. Morisawa, I. Kumagai, and F. Kanehiro, "Humanoid robot hrp-5p: An electrically actuated humanoid robot with high-power and wide-range joints," *IEEE Robotics and Automation Letters*, vol. 4, no. 2, pp. 1431–1438, 2019.
- [10] K. Choi, J. Kwon, T. Lee, C. Park, J. Pyo, C. Lee, S. Lee, I. Kim, S. Seok, Y.-J. Kim, *et al.*, "A hybrid dynamic model for the ambidex tendon-driven manipulator," *Mechatronics*, vol. 69, p. 102398, 2020.
- [11] Y.-J. Kim, J.-I. Kim, and W. Jang, "Quaternion joint: Dexterous 3-dof joint representing quaternion motion for high-speed safe interaction," *2018 IEEE/RSJ International Conference on Intelligent Robots and Systems (IROS)*, pp. 935–942, 2018.
- [12] T. Asfour, J. Schill, H. Peters, C. Klas, J. Bückner, C. Sander, S. Schulz, A. Kargov, T. Werner, and V. Bartenbach, "Armar-4: A 63 dof torque controlled humanoid robot," in *2013 13th IEEE-RAS International Conference on Humanoid Robots (Humanoids)*. IEEE, 2013, pp. 390–396.

- [13] D. V. Gealy, S. McKinley, B. Yi, P. Wu, P. R. Downey, G. Balke, A. Zhao, M. Guo, R. Thomasson, A. Sinclair, *et al.*, “Quasi-direct drive for low-cost compliant robotic manipulation,” in *2019 International Conference on Robotics and Automation (ICRA)*. IEEE, 2019, pp. 437–443.
- [14] N. G. Tsagarakis, G. Metta, G. Sandini, D. Vernon, R. Beira, F. Becchi, L. Righetti, J. Santos-Victor, A. J. Ijspeert, M. C. Carrozza, *et al.*, “icub: the design and realization of an open humanoid platform for cognitive and neuroscience research,” *Advanced Robotics*, vol. 21, no. 10, pp. 1151–1175, 2007.
- [15] S. Feng, E. Whitman, X. Xinjilefu, and C. G. Atkeson, “Optimization based full body control for the atlas robot,” in *2014 IEEE-RAS International Conference on Humanoid Robots*, 2014, pp. 120–127.
- [16] N. M. Bajaj, A. J. Spiers, and A. M. Dollar, “State of the art in artificial wrists: a review of prosthetic and robotic wrist design,” *IEEE Transactions on Robotics*, vol. 35, no. 1, pp. 261–277, 2019.
- [17] D. Shah, Y. Wu, A. Scalzo, G. Metta, and A. Parmiggiani, “A comparison of robot wrist implementations for the icub humanoid,” *Robotics*, vol. 8, no. 1, p. 11, 2019.
- [18] S. Rader, L. Kaul, P. Weiner, and T. Asfour, “Highly integrated sensor-actuator-controller units for modular robot design,” in *IEEE International Conference on Advanced Intelligent Mechatronics (AIM)*, 2017, pp. 1160–1166.
- [19] A. Toedtheide, J. Kühn, E. P. Fortunić, and S. Haddadin, “An integrated, force-sensitive, impedance controlled, tendon-driven wrist: Design, modeling, and control,” in *2020 IEEE-RAS 20th International Conference on Humanoid Robots (Humanoids)*. IEEE, 2021, pp. 25–32.
- [20] “Dexterous hand series: The world’s most dexterous humanoid robot hands,” <https://www.shadowrobot.com/dexterous-hand-series/>, accessed: 2022-01-31.
- [21] W. Friedl, H. Höppner, F. Petit, and G. Hirzinger, “Wrist and forearm rotation of the dlr hand arm system: Mechanical design, shape analysis and experimental validation,” in *2011 IEEE/RSJ International Conference on Intelligent Robots and Systems*. IEEE, 2011, pp. 1836–1842.
- [22] A. Albers, S. Brudniok, J. Ottmad, C. Sauter, and K. Sedchaicharn, “Upper body of a new humanoid robot—the design of armar III,” in *2006 6th IEEE-RAS International Conference on Humanoid Robots*. IEEE, 2006, pp. 308–313.
- [23] A. Albers, J. Ottmad, and C. Sander, “Development of a new 2 dof lightweight wrist for the humanoid robot armar,” in *Advances in Robot Manipulators*. IntechOpen, 2010.
- [24] “HexGen HEX500-350HL,” [https://www.newport.com/mam/celum/](https://www.newport.com/mam/celum/celum_assets/resources/HXP1000_Data_Sheet.pdf)
- [celum_assets/resources/HXP1000_Data_Sheet.pdf](https://www.newport.com/mam/celum/celum_assets/resources/HXP1000_Data_Sheet.pdf), accessed: 2022-07-14.
- [25] J.-P. Merlet, C. Gosselin, and T. Huang, “Parallel mechanisms,” in *Springer handbook of robotics*. Springer, 2016, pp. 443–462.
- [26] A. V. Sureshbabu, J. H. Chang, L. Fiorio, A. Scalzo, G. Metta, and A. Parmiggiani, “A parallel kinematic wrist for the r1 humanoid robot,” in *2017 IEEE International conference on advanced intelligent mechatronics (AIM)*. IEEE, 2017, pp. 1215–1220.
- [27] J. Lemburg, J. de Gea Fernández, M. Eich, D. Mronga, P. Kampmann, A. Vogt, A. Aggarwal, Y. Shi, and F. Kirchner, “Aila-design of an autonomous mobile dual-arm robot,” in *2011 IEEE International Conference on Robotics and Automation*. IEEE, 2011, pp. 5147–5153.
- [28] Y.-J. Kim, Y. Lee, J. Kim, J.-W. Lee, K.-M. Park, K.-S. Roh, and J.-Y. Choi, “Roboray hand: A highly backdrivable robotic hand with sensorless contact force measurements,” in *2014 IEEE International Conference on Robotics and Automation (ICRA)*, 2014, pp. 6712–6718.
- [29] J. Sofka, V. Skormin, V. Nikulin, and D. Nicholson, “Omni-wrist III—a new generation of pointing devices. part i. laser beam steering devices—mathematical modeling,” *IEEE transactions on aerospace and electronic systems*, vol. 42, no. 2, pp. 718–725, 2006.
- [30] H. Song, Y.-S. Kim, J. Yoon, S.-H. Yun, J. Seo, and Y.-J. Kim, “Development of low-inertia high-stiffness manipulator limbs2 for high-speed manipulation of foldable objects,” *2018 IEEE/RSJ International Conference on Intelligent Robots and Systems (IROS)*, pp. 4145–4151, 2018.
- [31] “Robotic Surrogate III,” <https://www.anthrobot.com/surrog.III/>, accessed: 2022-07-14.
- [32] D. C. Boone and S. P. Azen, “Normal range of motion of joints in male subjects.” *JBJS*, vol. 61, no. 5, pp. 756–759, 1979.
- [33] C. Mandery, Ö. Terlemez, M. Do, N. Vahrenkamp, and T. Asfour, “The kit whole-body human motion database,” in *2015 International Conference on Advanced Robotics (ICAR)*. IEEE, 2015, pp. 329–336.
- [34] D. F. Machekposhti, N. Tolou, and J. Herder, “A fully compliant constant velocity universal joint,” in *International Design Engineering Technical Conferences and Computers and Information in Engineering Conference*, vol. 57120. American Society of Mechanical Engineers, 2015, p. V05AT08A014.
- [35] Y. Patel, P. George, *et al.*, “Parallel manipulators applications—a survey,” *Modern Mechanical Engineering*, vol. 2, no. 03, p. 57, 2012.
- [36] “Thk cross roller ring.” [Online]. Available: https://tech.thk.com/upload/catalog_claim/pdf/382-3G_CrossRollerRing.pdf